Comparative experimental and theoretical study on the molecular structure and spectroscopic properties of sideroxol isolated from *Sideritis stricta* and its electronic properties

Akın Azizoglu[a]*, Züleyha Özer[b], Sema Çarıkçı[c], and Turgut Kılıç[d]

[a] *University of Balıkesir. Faculty of Arts and Sciences. Department of Chemistry. TR 10145. Balıkesir. Turkey*

[b] *University of Balıkesir, Altınoluk Vocational School, TR 10870, Balıkesir, Turkey*

[c] *Izmir University of Democracy, Vocational School, TR 35140, Izmir, Turkey*

[d] *University of Balıkesir, Necatibey Faculty of Education, Department of Science Education, TR 10100, Balıkesir, Turkey*

azizoglu@balikesir.edu.tr

Keywords: *Sideritis, diterpene, DFT, GIAO*

Sideroxol, a kaurene diterpene, was obtained from the acetone extract of *Sideritis stricta* plant. The ground-state molecular geometry, vibrational frequencies, and NMR chemical shifts were also investigated by using various density functional theories and Pople basis sets. The computed geometries are in good conformity with the experimental data. The comparison between theory and experiments indicates that B3LYP and M06 methods with the 6-31G(d) basis set are able to provide satisfactory results for predicting vibrational and NMR properties. There seems to be no significant effect of addition of diffuse and polarization functions in the basis set used herein.

Introduction

The genus *Sideritis* belongs to the Labiateae family, which incorporates a wide variety of plants with biological and medical applications [1,2]. This genus comprises more than 150 perennial and annual vegetal species widely distributed in the Mediterranean area [3]. *Sideritis* species are widespread used against gastrointestinal disorders, such as stomachache, indigestion and flatulence, to alleviate the symptoms of common colds including fever, flu, sore throat, and bronchitis as well as a tonic and diuretic remedy [4-6]. The chemical components found in *Sideritis* genus include terpenes, diterpenes, flavonoids, essential oil, iridoids, coumarins, lignanes and sterols [7]. Particularly, diterpenoids are the largest and most widespread class of secondary metabolites isolated from dichloromethane and acetone extracts of medicinal plants [8].

Sideroxol (ent-7α.18-dihydroxy-15β.16β-epoxykaurane, **Figure 1**), a kaurene diterpenoid, is an important compound that has many derivatives with a wide range of interesting

properties, such as antifeedant, antioxidant, anticholinesterase, antibacterial and antifungal activities [9,10]. It can be isolated from *Sideritis arguta, S. leptoclada, S. gulendami, S. rubiflora, S. congesta, S. dichotoma,* and *S. stricta* [11,12].

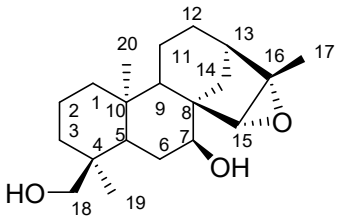

Figure 1. Structure and atom numbering scheme of sideroxol

In recent years, Density Functional Theory (DFT) methods have been increasingly applied to representative biological active compounds aiming to elucidate their molecular structures and electronic properties, thus contributing to the recognition of structure activity relationships and to the understanding of the properties and behavior of the system [13-16]. Especially DFT has become the dominant computational method for dealing with organic molecules isolated from plants [17,18].

Vibrational analyses of organic molecules extracted from aromatic and medicinal plants are necessary to ensure detailed information about their geometrical, vibrational and electronic properties [19,20]. To the best of our knowledge no theoretical calculations of sideroxol have been reported so far. It may be due to difficulties in interpreting the computational results because of their complexity and low symmetry. Hence, we wish to report the optimal geometry and the detailed vibrational spectrum of sideroxol with the help of theoretical and experimental techniques. Moreover, the gauge-including atomic orbital (GIAO) ^{1}H and ^{13}C chemical shift computations have been analyzed using various DFT methods. The spectroscopic constants obtained by DFT calculations have been compared with the corresponding experimental values.

Experimental part

Materials and Instruments

Unless otherwise specified, solvents and chemicals purchased from Merck Company were used as received without further purification. The FTIR spectrum of sideroxol was recorded using IR grade KBr disks on a Perkin–Elmer 1600 Series FT-IR spectrophotometer. Pellets were scanned at 4.0 cm^{-1} resolution in the spectral range of 4000–400 cm^{-1} at room temperature. ^{1}H- and ^{13}C-NMR spectra were obtained in $CDCl_3$ by using Varian 500 MHz NMR spectrometer.

Plant material

Sideroxol ($C_{20}H_{32}O_3$) was isolated from *Sideritis stricta Boiss. & Heldr.* (Lamiaceae), collected in July 2019 from Termesos National Park (Antalya Province. Turkey). The plant was identified by Prof. Dr. Tuncay Dirmenci from University of Balıkesir, Turkey.

Extraction and isolation

The aerial parts of *Sideritis stricta* were dried at room temperature and (1.5 kg) were extracted with acetone at room temperature for three days. The resulting solution was distilled (40 °C) under reduced pressure to give the acetone extract (31.8 g). Column adsorption chromatography was carried out with silica gel 60. Column length and diameter were adapted according to sample quantity. Elution was started with n-hexane and continued with gradients of dichloromethane, acetone and methanol. Fractions were controlled via Thin Layer Chromatography (TLC) techniques, and similar fractions were combined. These fractions were subjected to further small column chromatographies, controlled by TLC again. From the acetone extract, sideroxol was isolated. The structures of other isolated diterpenoids, 7-epicandicandiol, linearol, foliol, sideridiol, and siderol were confirmed by comparison with literature data [11,12].

Theoretical part

For all the theoretical computations, performed by using the GAUSSIAN 09 package program [21], gaseous phase conditions have been considered at 1 atm pressure and at a temperature of 298 K. Initial molecular geometry, generated from standard geometrical parameters, was minimized without any constraint on the potential energy surface at the PM3 level. This geometry was then optimized again at the B3LYP/6-31+G(d), M06/6-31+G(d), mPW1PW91/6-31+G(d), B3LYP/6-31++G(d.p), M06/6-31++G(d.p), and mPW1PW91/6-31++G(d.p) levels [22]. The obtained structural parameters were subjected to the vibrational frequency calculations resulting in IR peaks together with intensities at the corresponding DFT levels. Moreover, the absolute assignments of ^{1}H and ^{13}C chemical shift values were computed subtracting the isotropic shielding tensor (in ppm) of each atom from the corresponding DFT/GIAO shielding tensor of the reference TMS, which was calculated from its optimized geometry at the related level and basis set of sideroxol. Vibrational frequency assignments and NMR analyses were achieved with a high degree of accuracy using the software package Gauss View 5.0 and GAUSSIAN 09 program [21].

Results and discussion

Structural analysis

The geometry optimization is a crucial step for the theoretical calculation of IR and NMR spectra of sideroxol because the molecular parameters are controlled by the geometry of the molecule. The optimized structure of sideroxol performed at the B3LYP/6-31++G(d.p) level is depicted in **Figure 2**. As usual for flexible molecules of this size, a large number of conformers will be obtained by using theoretical methods. In order to locate the preferred conformer of lowest energy for sideroxol, its X-

ray structural data was modeled, and then optimized without any constraints.

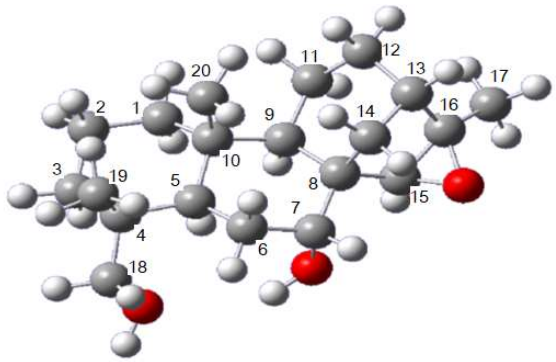

Figure 2. The optimized structure of sideroxol at the B3LYP/6-31++G(d.p) level (The white, red, and grey spheres represent hydrogen, oxygen, and carbon atoms, respectively).

The optimized geometric parameters (bond lengths. bond angles. and dihedral angles) are also listed in **Table 1**. Theoretical data were compared with the experimental X-ray structure reported by Kilic et al [23]. The theoretical bond lengths (C^8-C^{15}, C^8-C^{14}, and C^4-C^{18}) of sideroxol are determined to be 1.538, 1.554, and 1.550 Å at the B3LYP/6-31++G(d.p), 1.526, 1.542, and 1.537 Å at the M06/6-31++G(d.p), and 1.528, 1.544, and 1.541 Å at the mPW1PW91/6-31++G(d.p) levels. The latter are in much better agreement with experimental values of 1.532, 1.542, and 1.540 Å, respectively. On the other hand, M06 levels give poor structural data at the calculation of C-O bond lengths. The optimized C^{18}-O^{18}, C^7-O^7, C^{15}-O, and C^{16}-O bond lengths at the M06/6-31+G(d) level are computed to be 1.420, 1.424, 1.425, and 1.432 Å, respectively. In addition, the results of M06/6-31++G(d.p) method are found to be 1.420, 1.424, 1.425, and 1.431 Å, which tend to be shorter than the experimental values of 1.428, 1.465, 1.467, and 1.467 Å, respectively.

The correlation coefficient values (R^2) between experimental and theoretical bond lengths are calculated to be 0.968, 0.960, and 0.963 for B3LYP, M06, mPW1PW91 methods, respectively, with 6-31+G(d) basis set. After the addition of polarization and diffuse functions, they are calculated to be 0.966, 0.959, and 0.962 for B3LYP, M06, mPW1PW91 methods, respectively, with the 6-31++G(d.p) basis set. It can be said that addition of polarization and diffuse functions on hydrogen makes no appreciable change in structural parameters. Various calculated bond angles and dihedral angles of sideroxol are also found to be in satisfactory agreement with the reported standard values. Especially M06 levels give dihedral angles in excellent agreement with each other and also with the experimental values.

Table 1: Optimized structural parameters (bond length (Å), bond angle and dihedral angle (°)) of sideroxol

Bond length(Å)	Exp.	B3LYP		M06		mPW1PW91	
		6-31+G(d)	6-31++G(d.p)	6-31+G(d)	6-31++G(d.p)	6-31+G(d)	6-31++G(d.p)
C^{18}-O^{18}	1.428	1.436	1.436	1.420	1.420	1.424	1.424
C^{7}-O^{7}	1.465	1.440	1.440	1.424	1.424	1.427	1.427
C^{15}-O	1.467	1.445	1.446	1.425	1.425	1.432	1.432
C^{16}-O	1.467	1.451	1.450	1.432	1.431	1.437	1.437
C^{16}-C^{17}	1.492	1.506	1.506	1.495	1.495	1.499	1.499
C^{8}-C^{15}	1.532	1.538	1.538	1.526	1.526	1.528	1.528
C^{13}-C^{16}	1.526	1.533	1.534	1.522	1.522	1.525	1.526
C^{4}-C^{18}	1.540	1.550	1.550	1.536	1.537	1.541	1.541
C^{8}-C^{14}	1.542	1.554	1.554	1.542	1.542	1.543	1.544
C^{13}-C^{14}	1.544	1.542	1.541	1.530	1.530	1.533	1.533
C^{15}-C^{16}	1.478	1.470	1.470	1.460	1.460	1.465	1.465
H^{15}-C^{15}	0.955	1.087	1.087	1.092	1.091	1.086	1.086
C^{7}-H^{7}	1.042	1.099	1.099	1.106	1.105	1.099	1.099
O^{18}-H	0.988	0.968	0.965	0.965	0.962	0.964	0.961
C^{18}-H^{18a}	0.940	1.090	1.098	1.104	1.103	1.098	1.098
C^{18}-H^{18b}	0.976	1.100	1.099	1.105	1.103	1.099	1.099
R^2 values	-	*0.968*	*0.966*	*0.960*	*0.959*	*0.963*	*0.962*
Bond angle(°)							
C^{18}-O^{18}-H	117.3	109.8	108.9	109.1	109.1	108.8	108.8
C^{7}-O^{7}-H	119.5	109.4	109.4	109.4	109.5	109.1	109.2
H^{18a}-C^{18}-O^{18}	108.95	109.5	109.7	110.3	110.2	109.8	109.9
H^{18b}-C^{18}-O^{18}	110.4	109.9	110.0	110.1	110.5	110.2	110.3
H^{7}-C^{7}-O^{7}	109.3	107.9	108.1	108.5	108.6	108.1	108.2
C^{15}-O-C^{16}	60.47	61.01	61.0	61.46	61.48	61.39	61.41
C^{16}-C^{15}-O	59.76	59.67	59.64	59.49	59.46	59.47	59.44
C^{15}-C^{16}-O	59.77	59.31	59.33	59.04	59.05	59.13	59.15
C^{17}-C^{16}-O	115.1	115.3	115.4	115.6	115.7	115.6	115.7
C^{13}-C^{14}-C^{8}	100.9	102.2	102.1	102.1	102.1	102.2	102.2
C^{14}-C^{13}-C^{16}	103.8	102.6	102.6	102.6	102.5	102.5	102.5
C^{14}-C^{8}-C^{15}	102.3	100.4	100.4	100.6	100.7	100.5	100.5
C^{15}-C^{16}-C^{17}	125.1	125.6	125.6	125.3	125.3	125.4	125.4
R^2 values	-	*0.980*	*0.978*	*0.978*	*0.978*	*0.977*	*0.977*
Dihedral angle (°)							
C^{19}-C^{4}-C^{18}-O^{18}	-179.8	-167.8	-168.3	-167.9	-168.2	-167.0	-167.4
C^{8}-C^{7}-O^{7}-H	-174.5	-144.8	-146.3	-148.6	-147.8	-140.4	-139.9
C^{6}-C^{7}-O^{7}-H	-61.58	-22.06	-23.64	-26.35	-25.47	-18.06	-17.53
C^{14}-C^{8}-C^{15}-O	37.82	38.78	38.68	38.78	38.68	38.49	38.36
C^{14}-C^{13}-C^{16}-O	-37.57	-36.89	-36.85	-36.51	-36.5	-36.72	-36.68
C^{17}-C^{16}-C^{15}-O	100.9	100.8	100.8	101.2	101.2	101.1	101.2
C^{8}-C^{15}-C^{16}-C^{17}	-153.9	-151.7	-151.7	-151.2	-151.1	-151.4	-151.4
R^2 values	-	*0.980*	*0.981*	*0.985*	*0.984*	*0.975*	*0.974*

Spectral analysis

FT-IR spectroscopy is one of the most useful tools for identification of the novel compounds in terms of both experimental and computational studies. Herein, a frequency calculation analysis has been performed to obtain the spectroscopic signature of the title molecule, which belongs to *C1* point group symmetry. The assignments of the experimental frequencies are based on the observed band frequencies in the IR

spectrum of this species confirmed by establishing "one to one" correlation between experiment and theory. In total there are 159 vibrational normal modes about 52 to 3919 cm^{-1} at the DFT levels applied herein. The FT-IR experimental and theoretical spectra of sideroxol are depicted in **Figure 3**. The correlation between the calculated and experimental spectra seems to be very good.

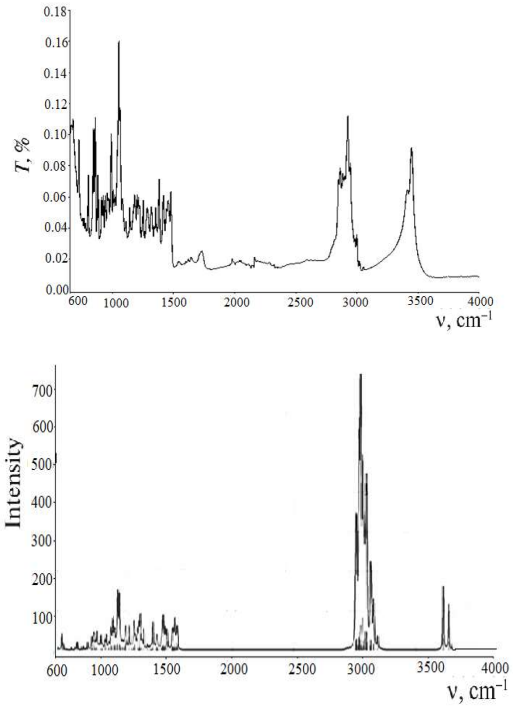

Figure 3. Experimental (**top**) and theoretical (**bottom**) FT-IR spectra at the B3LYP/6-31+G(d) level.

The main focus of the present investigation is the proper assignment of the experimental frequencies to the various vibrational modes of sideroxol in corroboration with the computed harmonic frequencies at various DFT levels. **Table 2** lists selected and detailed description of the assignments of vibrational wavenumbers of sideroxol.

The region between 2800 cm^{-1} and 3000 cm^{-1} contains IR bands originated from C-H stretching vibrations [24]. Experimental stretching vibrations are observed at 2862 cm^{-1} and 2927 cm^{-1}, and corresponds to the calculated vibrational wavenumbers located at 2977 cm^{-1} and 2978 cm^{-1}. These peaks are related with the stretching vibrations of $C^{18}H_2$ and $C^{7}H$, respectively. The symmetrical stretching vibrations of methyl groups appear in the region between 3021 cm^{-1} and 3064 cm^{-1} (C^{19}), 3027cm^{-1} and 3071 cm^{-1} (C^{17}), 3057 cm^{-1} and 3097 cm^{-1} (C^{20}). The asymmetrical stretchings are also found theoretically in the regions 3095 cm^{-1} - 3187 cm^{-1} (C^{19}), 3098 cm^{-1} - 3140 cm^{-1} (C^{17}), and 3129 cm^{-1} - 3167 cm^{-1} (C^{20}).

The C-O stretching vibrations are expected to be observed around 1200 cm^{-1} for natural diterpene products [25, 26]. The title molecule has two CO symmetrical stretching vibrations. Experimental CO symmetric vibrations of the title molecule are observed at 1051 cm^{-1} and 1140 cm^{-1} for $C^{18}O$ and $C^{7}O$, respectively. The corresponding theoretical frequencies are found to be 1061, 1058, 1112, 1108, 1094, and 1090 cm^{-1} for $C^{18}O$, whereas those for $C^{7}O$ are 1074, 1070, 1127, 1123, 1101, and 1097 cm^{-1} at the B3LYP, M06, and mPW1PW91 with 6-31+G(d) and 6-31++G(d.p) basis sets, respectively. Epoxide group (C^{15}-O-C^{16}) of title molecule displays no easily

distinguishable infrared band experimentally. However, the medium peaks around 841-912 cm^{-1} correspond to epoxide ring vibrations observed in the theoretical spectra at DFT levels studied herein.

Table 2. Selected experimental and calculated vibrational wavenumbers and their assignments for sideroxol

Exp.	B3LYP		M06		mPW1PW91		Approximate description
	6-31+G(d)	6-31++G(d.p)	6-31+G(d)	6-31++G(d.p)	6-31+G(d)	6-31++G(d.p)	
1051.1	1061.4	1058.2	1112.8	1108.7	1094.4	1089.9	C-O stretching (C^{18})
1139.9	1074.5	1069.9	1127.5	1122.7	1101.1	1096.7	C-O stretching (C^{7})
	1108.7	1081.8	1193.3	1187.3	1186.9	1193.1	C-H wagging (C^{15})
1283.8	1310.5	1301.9	1293.4	1220.1	1320.2	1300.6	CH_2 twisting (C^{18})
1316.3	1328.8	1318.6	1324.3	1308.5	1334.6	1324.8	CH_2 wagging (C^{14})
1352.4	1350.6	1339.2	1336.6	1326.2	1358.7	1331.8	CH_2 wagging (C^{6})
1381.0	1383.7	1372.9	1378.6	1369.2	1381.7	1385.4	C-H wagging (C^{7})
1415.3	1432.4	1416.7	1417.5	1401.4	1434.6	1416.6	CH_3 wagging (C^{17})
1454.8	1449.9	1437.4	1435.4	1423.6	1455.5	1443.1	CH_2 wagging(C^{18})
	1452.1	1436.6	1397.2	1408.7	1420.8	1404.6	CH_3 wagging(C^{20})
1477.6	1462.8	1455.4	1516.9	1509.5	1487.2	1474.7	C^{15}-C^{16} symmet. stretching
	1519.3	1501.5	1488.4	1469.1	1514.3	1496.2	CH_3 scissoring (C^{17})
	1526.2	1505.9	1493.3	1472.9	1526.4	1504.6	CH_3 scissoring (C^{19})
	1539.0	1522.6	1503.1	1487.5	1543.9	1527.1	CH_2 scissoring (C^{18})
1731.6	1545.8	1531.7	1524.6	1503.1	1553.9	1531.1	CH_3 scissoring (C^{20})
2926.7	3007.7	3001.3	2980.8	2976.7	3030.4	3023.5	CH_2 symmetrical stretching (C^{18})
2862.6	3013.7	3008.9	2979.8	2978.1	3040.8	3036.8	C-H symmetrical stretching (C^{7})
	3038.9	3033.1	3025.2	3021.0	3063.8	3059.9	CH_3 symmetrical stretching (C^{19})
	3040.9	3037.9	3022.5	3022.7	3068.4	3064.9	CH_2 asymmetrical stretching (C^{18})
	3041.9	3037.7	3030.2	3027.1	3071.6	3066.6	CH_3 symmetrical stretching (C^{17})
	3076.4	3069.9	3063.3	3057.9	3097.3	3089.2	CH_3 symmetrical stretching (C^{20})
	3081.4	3081.0	3080.0	3079.9	3114.1	3113.7	CH_2 asymmetrical stretching (C^{6})
	3095.6 3156.1	3096.1 3153.3	3096.7 3152.3	3097.6 3151.2	3130.6 3187.2	3130.7 3183.2	CH_3 asymmetrical stretching (C^{19})
	3098.8	3099.1	3129.4	3131.0	3139.8	3139.5	CH_3 asymmetrical stretching (C^{17})
	3134.7	3134.2	3141.3	3129.6	3167.0	3165.6	CH_3 asymmetrical stretching (C^{20})
	3187.5	3181.6	3152.7	3150.9	3213.6	3208.0	C-H symmetrical stretching (C^{15})
3447.4	3725.7	3798.3	3802.5	3865.0	3776.9	3845.3	O-H symmetrical stretching (C^{7})
3447.4	3769.8	3845.1	3850.4	3919.1	3837.2	3911.7	O-H symmetrical stretching (C^{18})
-	*0.988*	*0.983*	*0.974*	*0.970*	*0.979*	*0.975*	*R^2 values*

The O-H vibration occurs generally in range 3700-3550 cm^{-1} [27]. The title compound has two OH groups. The DFT theoretical values between 3726 cm^{-1} and 3919 cm^{-1} are assigned to

the OH group vibrations, and the FT-IR band observed at 3447 cm^{-1} in the spectra agrees with the experimental value of stretching O-H group attached to the C^{18}.

The ring stretching vibrations are very important due to the characteristic nature in the IR spectrum. The C-C stretching vibrations of the ring usually occur in the range 1625-1400 cm^{-1}. The symmetrical C-C stretching vibration attached to C^{15}-C^{16} was experimentally assigned to 1478 cm^{-1}, whereas the B3LYP, M06, and mPW1PW91 with 6-31+G(d) and 6-31++G(d.p) basis sets gave 1463, 1455, 1517, 1510, 1487, and 1475 $cm^{-1,}$, respectively.

To make general comparison with experimental values, we obtained the correlation graphics, from which the correlation factors (R^2) of computational and experimental frequencies are found to be 0.988, 0.983, 0.974, 0.970, 0.979, and 0.975, at B3LYP, M06, and mPW1PW91 methods with the 6-31+G(d) and 6-31++G(d.p), respectively. Hence, the results of B3LYP method with the 6-31+G(d) basis set give the best fit with experimental values.

Generally, the theoretical frequencies are slightly higher than the observed values for the majority of the normal modes. Two factors may be responsible for the discrepancies between the experimental and calculated spectra of sideroxol. The first is explained by the environment and the second reason for these discrepancies is the fact that the experimental value is an anharmonic frequency in the solid phase while the calculated value is a harmonic one in the gaseous phase [28].

NMR spectroscopy constitutes an extremely useful tool for the determination of molecular electronic structure and structural information [29]. Recently, the comparison of theoretical NMR parameters with the respective experimental data for organic molecules extracted from aromatic and medicinal plants has also become a common practice for the determination of the correct arrangement of atoms in a molecule [18,30]. It is reported that there are very good correlations between experimental and theoretical magnetic properties (NMR nuclear shielding and spin-spin coupling constants), which are obtained with the GIAO approach by using ab-initio and DFT calculations. The comparisons between calculated and experimental values of NMR chemical shifts can be used to predict the extent of the agreement of the predicted geometric structure with respect to the real structure of molecule. Hence, the theoretical methods, such as the density functional theory (DFT) method have become the dominant computational tools for dealing with natural organic molecules [31]. The GIAO ^{1}H- and ^{13}C-NMR chemical shift values (with respect to TMS) have been calculated using DFT methods with 6-31+G(d) and 6-31++G(d.p) basis sets in the gaseous phase. The results are reported in Tables 3 and 4. Experimental DEPT spectrum of sideroxol was also shown in **Figure 4**. The correlation values of

experimental and theoretical ^{1}H- and ^{13}C-NMR chemical shifts are found to be 0.769 and 0.973 for the B3LYP/6-31+G(d), 0.813 and 0.967 for the B3LYP/6-31++G(d.p), 0.901 and 0.857 for the M06/6-31+G(d), 0.879 and 0.952 for the M06/6-31++G(d.p), 0.863 and 0.942 for the mPW1PW91/6-31+G(d), 0.794 and 0.928 for the mPW1PW91/6-31++G(d.p). Therefore, the M06 and B3LYP methods with 6-31+G(d) basis set have shown a better fit with experimental data than other DFT methods in evaluating ^{1}H and ^{13}C chemical shifts, respectively.

Table 3. Experimental and calculated ^{1}H-NMR chemical shifts (GIAO method) of sideroxol

		$\delta_{calc.}$ (ppm)					
Atom	$\delta_{exp.}$ **(ppm)**	**B3LYP**		**M06**		**mPW1PW91**	
		6-31+G(d)	6-31++G(d.p)	6-31+G(d)	6-31++G(d.p)	6-31+G(d)	6-31++G(d.p)
H^{1a}		1.74	2.07	1.66	2.48	1.76	2.09
H^{1b}		0.87	1.10	0.61	0.82	0.82	1.09
H^{2a}		1.51	1.95	1.04	1.45	1.49	1.93
H^{2b}		1.25	1.65	1.00	1.37	1.22	1.63
H^{3a}		0.99	1.32	1.28	1.61	1.84	2.10
H^{3b}		1.89	2.16	1.79	1.12	1.01	1.32
H^{5}		2.12	2.51	1.82	1.93	2.04	2.39
H^{6a}		1.53	1.97	1.49	1.90	1.44	2.94
H^{6b}		1.45	1.84	1.62	1.98	1.48	1.84
H^{7}	4.79	3.83	4.19	3.95	4.07	3.73	4.10
H^{9}		1.65	2.02	1.24	1.70	1.59	1.90
H^{11a}		1.27	1.64	1.11	1.54	1.24	1.65
H^{11b}		1.53	1.88	1.33	1.85	1.45	1.80
H^{12a}		1.50	1.77	1.10	1.01	1.48	1.78
H^{12b}		1.50	1.87	1.32	1.49	1.50	1.82
H^{13}		1.86	2.32	1.45	1.46	1.80	2.28
H^{14a}		1.07	1.39	0.97	1.09	1.07	1.38
H^{14b}		1.12	1.47	1.01	1.45	1.09	1.50
H^{15}		3.13	3.56	2.60	3.17	3.03	3.44
H^{17a}	1.40	1.45	1.84	0.97	1.55	1.42	1.82
H^{17b}	1.40	1.51	2.09	1.25	1.65	1.44	1.94
H^{17c}	1.40	0.70	1.11	0.50	0.73	0.69	1.09
H^{18a}	2.96	2.90	3.32	2.61	3.09	2.89	3.30
H^{18b}	3.49	3.47	4.03	2.85	3.43	3.42	3.97
H^{19a}	1.04	-0.08	0.24	-0.01	0.53	-0.09	0.23
H^{19b}	1.04	0.54	0.98	0.54	1.12	0.59	1.02
H^{19c}	1.04	0.97	1.48	0.93	1.45	0.96	1.50
H^{20a}	0.69	0.97	1.32	0.80	1.07	0.93	1.35
H^{20b}	0.69	1.92	1.40	0.93	1.18	0.99	1.46
H^{20c}	0.69	0.76	0.99	0.62	0.88	0.80	1.09
OH^{7}		1.11	1.35	1.02	1.15	1.23	1.60
OH^{18}		0.50	0.99	0.57	0.89	0.44	0.93

Table 4. Experimental and calculated ^{13}C-NMR chemical shifts (GIAO method) of sideroxol

		$\delta_{calc.}$ (ppm)					
Atom	$\delta_{exp.}$ **(ppm)**	**B3LYP**		**M06**		**mPW1PW91**	
		6-31+G(d)	6-31++G(d.p)	6-31+G(d)	6-31++G(d.p)	6-31+G(d)	6-31++G(d.p)
C^1	40.29	34.59	33.86	34.09	34.45	29.23	28.25
C^2	17.76	14.03	12.66	14.48	12.53	8.24	7.06
C^3	35.63	29.83	28.29	31.90	29.30	24.48	23.06
C^4	36.27	32.59	32.90	29.89	30.84	24.81	25.34
C^5	39.28	31.34	30.35	31.64	30.84	24.54	23.58
C^6	26.91	20.75	19.06	21.75	20.14	15.43	14.47
C^7	71.31	65.63	63.56	63.76	61.87	58.53	56.23
C^8	46.10	44.25	44.20	44.33	46.45	36.57	35.77
C^9	46.09	40.20	38.35	40.16	40.27	33.69	32.23
C^{10}	39.47	35.08	34.30	32.47	32.50	27.04	26.31
C^{11}	18.07	14.40	12.87	13.51	10.17	8.55	7.06
C^{12}	27.56	23.09	21.70	23.09	21.17	17.34	13.36
C^{13}	39.47	36.01	33.09	32.31	37.17	29.44	26.73
C^{14}	31.36	26.59	26.11	26.12	21.66	20.83	20.04
C^{15}	63.77	56.78	55.50	57.52	55.71	49.76	48.89
C^{16}	71.23	53.77	54.20	50.47	51.11	46.71	47.12
C^{17}	14.10	8.29	6.34	11.94	10.30	3.71	1.93
C^{18}	71.23	62.99	61.75	66.56	65.63	56.98	56.12
C^{19}	17.15	10.72	8.77	15.05	12.98	6.27	4.51
C^{20}	14.16	11.18	9.47	17.25	13.30	7.03	5.93

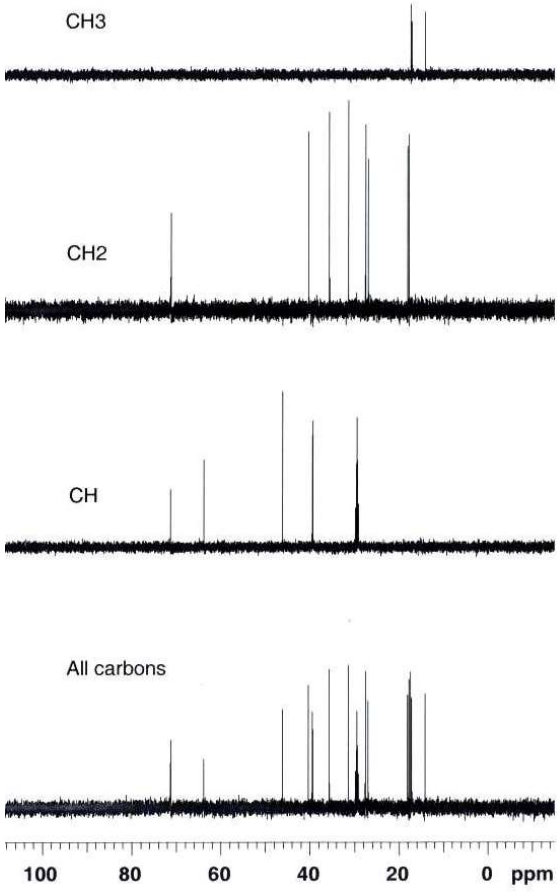

Figure 4. Experimental DEPT spectrum of sideroxol

The experimental signal at 4.79 ppm is also assigned to H atom attached to the C^7 atom. The theoretical one is found to be 3.83 ppm at B3LYP/6-31+G(d), 4.19 ppm at B3LYP/6-31++G(d.p), 3.95 ppm at M06/6-31+G(d), 4.07 ppm at M06/6-31++G(d.p), 3.73 ppm at mPW1PW91/6-31+G(d), and 4.10 ppm at mPW1PW91/6-31++G(d.p). The signals in the upfield corresponding to nine protons (1.40, 1.04, and 0.69 ppm) are easily assigned to the equivalent protons of the three methyl groups ($C^{17}H_3$, $C^{19}H_3$, and $C^{20}H_3$). Their calculated ^{1}H-NMR values are determined to be around 0.50-2.09 ppm for the $C^{17}H_3$, -0.09-1.50 ppm for the $C^{19}H_3$, and 0.62-1.92 ppm for the $C^{20}H_3$ with various DFT levels. **Tables 3** and **4** apparently show that calculated DFT data for sideroxol are

almost compatible with the experimental chemical shifts. Especially the B3LYP method shows a better agreement with experimental ^{13}C-NMR shift observation than other DFT levels used herein.

Frontier molecular orbital analysis

Frontier molecular orbital (FMO) theory in chemistry is an application of MO theory describing highest occupied MO (HOMO) and lowest unoccupied MO (LUMO) interactions that play an important role in the electric, optical and other properties, and chemical reactions [32]. Therefore, the highest occupied molecular orbital (HOMO) and lowest unoccupied molecular orbital (LUMO) were also investigated at the B3LYP/6-31++G(d.p) level (**Figure 5**). According to Koopman theorem [33], the HOMO energy is identical to the minus ionization potential when the orbital relaxation is neglected. The LUMO energy corresponds to the minus electron affinity. The HOMO-LUMO energy gap also explains the concluding charge transfer interaction within the molecule and is useful in determining molecular electrical transport properties. The HOMO–LUMO energy gap was calculated to be 6.1299 eV for sideroxol. The high value of the band gap was indicative of the stability of the compounds towards oxidation and reduction. A molecule with a high energy gap has low chemical reactivity and high kinetic stability, because it is energetically unfavorable to add an electron to the high-lying LUMO or to remove electrons from the low-lying HOMO [34]. The HOMOs are mainly located on the epoxide moieties, whereas LUMOs are substantially localized on the C^{18} atom, which is attached to hydroxyl group.

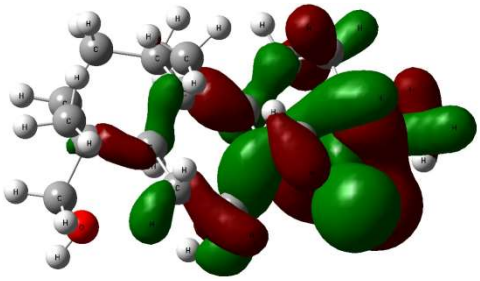

HOMO (-6.6782 eV)

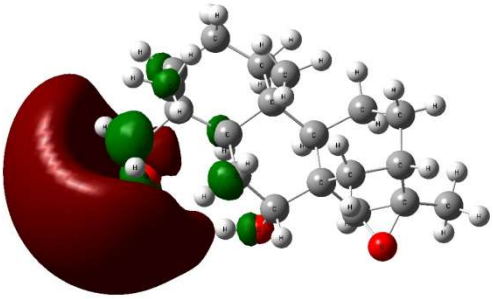

LUMO (-0.5483 *eV*)

Figure 5. HOMO and LUMO of sideroxol

Conclusions

In the current work, sideroxol has been isolated initially from *Sideritis Stricta*. and characterized as one of the chemical constituents of the traditionally used medicinal plant, based on detailed spectral studies including FT-IR, ^{1}H- and ^{13}C-NMR spectroscopy. Theoretical studies on the molecular structure (bond length. bond angle. dihedral angle), vibrational frequencies, chemical shifts, and electronic features of sideroxol have also been performed employing B3LYP, M06, and mPW1PW91 theories with both 6-31+G(d) and 6-31++G(d.p) basis sets.

The FT-IR spectrum has been interpreted using vibrational spectroscopic analysis. The calculated vibrational frequencies are found to be

in good agreement with the experimental values. In detail, experimental fundamentals are found to have slightly a better correlation for the B3LYP/6-31+G(d) level than other ones.

Proton and carbon nuclear magnetic resonance spectra (using GIAO method) are also found to be in good agreement with the experimental data. Results of the B3LYP theory with 6-31+G(d) basis set have shown a better fit with experimental data than other methods in evaluating ^{13}C-NMR chemical shifts. Moreover, the line of best fit, an output of regression analysis, between the calculated and the experimental ^{1}H-NMR chemical shifts has been defined by the M06/6-31+G(d) method.

The HOMO-LUMO gap value is computed to be 6.1299 eV for sideroxol. The HOMO represents the ability to donate an electron, whereas the LUMO acts for the ability to accept an electron. The calculated HOMO and LUMO energies can state that charge transfer occurs within the molecule.

Acknowledgements

The authors wish to thank TUBITAK (Grant Number: TBAG-105T430 and TBAG-113Z710) for generous financial supports. This work was also supported by Balikesir University Research Grant No. 2018/175. We would like to thank Prof. Dr. Tuncay Dirmenci (Balıkesir University) for plant identification. We are also grateful to the reviewers' valuable comments that improved our manuscript.

References

[1] Harley RM, Atkins S, Budantsev A, Cantino PD, Conn BJ, Grayer R, Harley MM, De Kok R, Krestovskaja T, Morales R. The Families and Genera of Vascular Plants. Berlin: Springer Verlag; 2004:167–275.

[2] Sağdiç O, Özcan M. Antibacterial activity of Turkish spice hydrosols. Food Control. 2003;14(3):141-143.

[3] Güner A, Aslan S, Ekim T, Vural M, Babaç MT. Türkiye Bitkileri Listesi (Damarlı Bitkiler), Istanbul: Nezahat Gökyiğit Botanik Bahçesi ve Flora Araştırmaları Derneği Publisher, 2012.

[4] Davis PH, Mill RR, Kit T. Flora of Turkey and the East Aegean Islands. Edinburgh: Edinburgh University Press; 1982;10.

[5] Küpeli E, Şahin FP, Yeşilada E, Çalış I, Ezer N. In vivo anti-inflammatory and antinociceptic activity evaluation of phenolic compunds from Sideritis stricta. Z. Naturforsch C, 2007;62:519-525.

[6] Güvenç A, Okada Y, Küpeli-Akkol E, Duman E, Okuyama T, Çalış I. Investigations of anti-inflammatory, antinociceptive, antioxidant and aldose reductase inhibitory activities of phenolic compounds from Sideritis brevibracteata. Food Chem. 2010;118(3):686-692.

[7] González-Burgos EE, Carretero ME, Gómez-Serranillos MP. Sideritis spp.: uses, chemical composition and pharmacological activities - a review. J Ethnopharmacol. 2011;135(2):209-225.

[8] Topcu G, Ulubelen A. Structure elucidation of organic compounds from natural sources using 1D and 2D NMR techniques. J. Mol. Struct., 2007;834:57-73.

[9] Topçu G, Ertas A, Dinçel D, Halfon B. Ent-kaurane diterpenoids isolated from Sideritis congesta. Phytochem Lett, 2011;4(4):436-439.

[10] Bondi ML, Bruno M, Piozzi F, Baser KHC, Simmonds MSJ. Diversity and antifeedant activity of diterpenes from Turkish species of Sideritis. Biochem. Syst. Ecol. 2000;28(4):299-303.

[11] Fraga BM. Phytochemistry and chemotaxonomy of Sideritis species from the Mediterranean region. Phytochem. 2012;76:7-24.

[12] Kilic T. Isolation and Biological Activity of New and Known Diterpenoids From Sideritis stricta Boiss. & Heldr. Molecules. 2006;11(4):257–262.

[13] Gamil MA, Sadeek SA, Zordok WA, El-Shwiniy WH. Spectroscopic, DFT modeling and biological study of some new mixed ligand metal complexes derived from gatifloxacin and pregabalin. J Mol Struct, 1209 (2020) 127941.

[14] Tkachenko VV, Farafonov VS, Tokarev VV, Tkachenko IG. Study of the effectiveness of various cannabinoid receptor 1 (CB1) agonists using molecular docking and molecular dynamics modeling. French Ukr. J. Chem. 2020;8(1):76-87.

[15] Bougossa I, Aggoun D, Ourari A, Berenguer R, Bouacida S, Morallon E. Synthesis and characterization of a novel non-symmetrical bidentate Schiff base ligand and its Ni(II) complex: electrochemical and antioxidant studies. Chem Papers, 2020;74:3825-3837.

[16] Kumar N, Chaudhary BPS, Singh D, Kumar D. Reduced graphene oxide contains a minimum of six oxygen atoms for higher dipolar strength: A DFT study. French Ukr. J. Chem. 2020;8(1):167-173.

[17] Costa ACDS, Carvalho SC, Silva NDF, Nascimento-Júnior AESD, Cruz JN, Neto AMDJC, Brasil DDSB, Silva-Júnior JOC, Ribeiro-Costa RM. Effect of chitosan/albendazole nanocarriers' solvation by molecular dynamics. Theor Chem Accounts. 2020;139(7):105.

[18] Costa RAD, Silva SG, Silva SDO, Cruz JN, Costas WAD, Brasil LSNDS, Silva RC, Santos CBR, Alves CN, BrasilL DDSB. Theoretical study via DFT for the prediction of 13C- and 1H-NMR data for two diterpenoids derived from the root of Salvia grandifolia. J. Serb. Chem. Soc. 2019;84(6):591-598.

[19] Minteguiaga M, Dellacassa E, Iramain MA, Catalan CAN, Brandan SA. FT-IR, FT-Raman, UV-Vis, NMR and structural studies of carquejyl acetate, a distinctive component of the essential oil from Baccharis trimera (less.) DC. (Asteraceae). J. Mol. Struct. 2019;1177:499-510.

[20] Citak S, Sagir Z O, Carikci S, Kilic T, Azizoglu A. Experimental and theoretical study on linearol isolated from Sideritis species. Rev. Roum. Chim. 2014;59(3-4):227-234.

[21] Frisch MJ, Trucks GW, Schlegel HB, Scuseria GE, Robb MA, Cheeseman JR, Scalmani G, BaroneV. Mennucci B. Petersson GA. Nakatsuji H, Caricato M. Li X. Hratchian HP. Izmaylov AF. Bloino J, Zheng G. Sonnenberg JL. Hada M. Ehara M. Toyota K, Fukuda R. Hasegawa J. Ishida M. Nakajima T. Honda Y, Kitao O. Nakai H. Vreven T. Montgomery JA Jr, Peralta JE, Ogliaro F, Bearpark M, Heyd JJ, Brothers E, Kudin KN, Staroverov VN, Keith T, Kobayashi R, Normand J, Raghavachari K, Rendell A, Burant JC, Iyengar SS, Tomasi J, Cossi M, Rega N, Millam JM, Klene M, Knox JE, Cross JB, Bakken V, Adamo C, Jaramillo J, Gomperts R, Stratmann RE, Yazyev O, Austin AJ, Cammi R, Pomelli C, Ochterski JW, Martin RL, Morokuma K, Zakrzewski VG, Voth GA, Salvador P, Dannenberg JJ, Dapprich S, Daniels AD, Farkas O, Foresman JB, Ortiz JV, Cioslowski J, Fox DJ. Gaussian 09. Revision A.02. Wallingford CT: Gaussian Inc.. 2010.

[22] Sholl DS, Steckel JA. Density Functional Theory: A Practical Introduction; New York: Wiley; 2009.

[23] Kilic T, Yildiz YK, Topçu G, Gören AC, Ay M, Bodige SG, Watson WH. X-ray analysis of sideroxol from Sideritis leptoclada. J. Chem Crystallogr. 2005;35(8):647–650.

[24] Silverstein RM, Bassler GC, Morrill TC. Spectrometric Identification of Organic Compounds. Chichester: John Wiley; 1991.

[25] Oliveira MM, Santos HS, Sena DM, Cruz BG, Teixeira AMR, et al. Vibrational spectra and DFT calculations of sonderianin diterpene. J. Mol. Struct. 2015;1099:226-231.

[26] Minaeva VA, Minaev BF, Baryshnikov GF, Romeyko OM, Pittelkow M. The FTIR spectra of substituted tetraoxa[8]circulenes and their assignments

based on DFT calculations. Vibrational Spect. 2013;65:147-158.

[27] Azizoglu A; Ozer Z; Kilic T. An experimental and theoretical study on siderol isolated from Sideritis species. Czech. Chem. Comm., 2011;76(2):95-114.

[28] Timouri A, Emami M, Chermahini AN, Dabbagh HA. Spectroscopic, quantum chemical DFT/HF study and synthesis of [2.2.1] hept-2′-en-2′-amino-N-azatricyclo [3.2.1.02,4] octane. Spectrochim. Acta Part A 2009;71(5):1749-1755.

[29] Balci M. Basic 1H- and 13C-NMR Spectroscopy. Amsterdam: Elsevier Science; 2005.

[30] Almeida B. Firme CL. et al. Experimental and NMR theoretical methodology applied to geometric analysis of the bioactive clerodane trans-dehydrocrotonin. J. Braz. Chem. Soc. 2014;25(4):629-638.

[31] Becke AD, Density-functional thermochemistry. V. Systematic optimization of exchange-correlation functionals. J. Chem. Phys. 1997;107:8554-8560.

[32] Fleming I. Frontier Orbitals and Organic Chemical Reactions. London: Wiley; 1976.

[33] Koopmans TA. Über die Zuordnung von Wellenfunktionen und Eigenwerten zu den Einzelnen Elektronen Eines Atoms. Physica 1934;1:104-113.

[34] Miar M, Shiroudi A, Pourshamsian K, Oliaey AR, Hatamjafari F. J. Chem. Res. 2021;45:147-158.